Reconstruction of Holocene Optimum paleoclimatic variations using long-chain *n*-alkanes and alkenones in sediments from Dabusu Lake, northeastern China

Ken Sawada[a]*, Makiko Ono[a], Hideto Nakamura[a, b], Shafi Mohammad Tareq[c, d]

[a] *Department of Earth and Planetary Sciences, Faculty of Science, Hokkaido University, N10W8, Kita-ku, Sapporo 060-0810, Japan.*

[b] *Department of Geosciences, Faculty of Science, Osaka City University, 3-3-138 Sugimoto, Sumiyoshi-ku, Osaka 558-8585, Japan.*

[c] *Department of Hydrospheric-Atmospheric Sciences, Graduate School of Environmental Studies, Nagoya University, Nagoya 464-8601, Japan.*

[d] *Department of Environmental Sciences, Jahangirnagar University, Dhaka 1342, Bangladesh*

*Corresponding author. Tel: +81-11-706-2733; fax: +81-11-746-0394.

E-mail address: sawadak@sci.hokudai.ac.jp

Quaternary International, Volume 550, Pages 27-38, 2020

https://doi.org/10.1016/j.quaint.2020.03.011

Abstract

Long-chain *n*-alkanes and alkenones were analyzed in sediments from Dabusu Lake, northeastern China, from ca. 7.2–4.5 kyr BP (the Holocene Optimum) and the present. Long-chain *n*-alkanes are derived from leaf waxes of terrestrial vascular plants and aquatic macrophytes. Using *n*-alkane proxies such as *P*aq and average chain length (ACL) indices, variations in paleovegetation were reconstructed. The *P*aq values were generally low, indicating that aquatic macrophytes were a minor floral component in Dabusu Lake. The ACL data indicated that forest/grassland mixed vegetation occurred around the lake. From the alkenone distribution patterns (C_{37}/C_{38}, C_{40}/C_{37}, and $\%C_{37:4}$ ratios), the main alkenone producers were inferred to be Group II producers, especially *Ruttnera lamellosa*. We estimated water temperatures based on alkenone unsaturation indices (U^{K}_{37} and $U^{K''}_{37}$) using the temperature calibrations obtained from culture strains of *R. lamellosa*. The variation pattern of the $U^{K''}_{37}$-based water temperatures was almost similar to that of the U^{K}_{37}-based pattern, although some spikes differed between the temperatures based on the two indices. The $U^{K''}_{37}$-based water temperatures were lower from 7.2 to 6.2 kyr BP, and subsequently increased after 6.2 kyr BP. The alkenone-based temperatures were highest from 5.5 to 5.3 kyr BP, indicating that this maximal stage was the Holocene Thermal Maximum in the Dabusu region. The markedly decreasing spikes of $U^{K''}_{37}$-based water temperatures in our study likely corresponded to the cooling events during the Holocene Optimum, as previously reported, especially Asian monsoon events (AM) 1 and Bond event 4 (BE4). Also, the increasing spike (7.2 kyr BP) in temperatures was possibly associated with the warming regime just after AM2. Moreover, the rapid increasing spikes of alkenone-based temperatures corresponded to those of *P*aq at 7.2 kyr BP (just after AM2) and 6.4 kyr BP. These results imply that the rapid warming reconstructed using alkenone-based temperatures might have resulted in increased precipitation around the lake at these ages,

especially just after the AM2 cooling.

1. Introduction

Dabusu Lake is a continental saline lake located in the west of Qian'an County, Jilin Province, in northeastern China (Fig. 1). The present climate around the lake is temperate, seasonally variable, and affected by the East Asian monsoon (EAM) system. In winter, cold air mass expands, and the northeasterly wind flow is dominant on the continent, whereas in summer, a warm and moist oceanic air mass is widely distributed. The Westerlies also influence summer and winter monsoons. Paleoenvironmental investigations of sediments from northern Chinese lakes such as Dabusu Lake provide an understanding of several millennial-scale continental climatic systems associated with the EAM, especially winter monsoons. Several millennial-scale variations in the Chinese climate have been reported, and particularly, paleovegetation changes were reconstructed under warmer conditions during the Holocene. Xiao et al. (2004) reported the variations in paleovegetation recorded by pollen assemblages and concentrations in sediments from Daihai Lake (north-central China) during the Holocene. Their vegetation records indicated that the climate in north-central China from 7,900 to 4,450 cal yr BP was warm and moist. This time period corresponds to the Holocene Optimum, and the climatic maximum (the Holocene Thermal Maximum [HTM]), which was characterized by the warmest temperature and highest precipitation, occurred ca. 6,010–5,100 cal yr BP. Zhao and Yu (2012) synthesized time-series data for vegetation and climate using pollen analysis for the monsoonal margin region of China during the Holocene, and demonstrated that the general climatic variation pattern in the margin region was slightly humid in the early Holocene, mostly arid in the middle Holocene, and arid in the late Holocene, although there was regional variability, as reflected by

vegetation change. Moreover, high-resolution oxygen isotope ($\delta^{18}O$) records of stalagmites from Dongge Cave (southern China) clearly indicated eight weak monsoon events, of which six events likely corresponded to the North Atlantic ice-rafting events (Bond events 0–5; Bond et al., 2001) even during the Holocene Optimum (Dykoski et al., 2005; Wang et al., 2005). Also, Li et al. (2011) demonstrated that the weak monsoonal events, including the Bond events, could be observed in the pollen records from Jingbo Lake (northeastern China). In Dabusu Lake, climatic variations have been roughly reconstructed using carbon isotope ratios ($\delta^{13}C$) of organic matter, carbonate contents, and carbonate $\delta^{18}O$ in the sediments over the last ~15,000 years (Shen et al. 2004). However, bulk chemical records such as organic $\delta^{13}C$ and carbonate $\delta^{18}O$ are less useful as paleotemperature proxies in lake environments.

Recently, lipid biomarker studies have shown that powerful paleoenvironmental and paleoclimatic analyses of lake settings can be performed by investigating the amount and type of organic matter in lacustrine sediments. In the last decade, paleothermometry using long-chain alkenones was increasingly applied to lacustrine sediments to reconstruct lacustrine water and air temperatures in the continental environment (Liu et al., 2006; Randlett et al., 2014; Wang et al., 2015). Also, long-chain *n*-alkanes, which are derived from plant wax, have been commonly used to reconstruct paleoenvironments and paleovegetation in the intercontinental area (e.g., Fisher et al., 2004; Zhang et al., 2004; Boot et al., 2006; Regnery et al., 2013). In Chinese areas, the variations in paleovegetation during the Holocene and Pleistocene glacial/interglacial periods have been reconstructed using long-chain *n*-alkane proxies, including carbon and hydrogen isotope analyses of these *n*-alkanes (Zhang et al., 2004; Li et al., 2016).

In the present study, we analyzed biomarkers such as long-chain *n*-alkanes and alkenones to reconstruct the paleovegetation and paleotemperature around the lake, respectively. From these biomarker records, we were able to describe the millennial-

scale variations in the Holocene paleoclimate in northeastern China.

2. Material and methods

2.1. Study area and samples

Dabusu Lake is located in the center of the belt of the Songliao Basin, China. The lake has a 230-km^2 catchment area, extending from the southeast to the northeast (10 km long and 6 km wide). There is no continuous stream input into Lake Dabusu, nor an outlet from the lake; thus, the water level is controlled by the precipitation/evaporation ratio. Sites DBA (44°47'15.8" N, 123°41'12" E) and DBB (44°46'54.6" N, 123°39'3.4" E) are located on the eastern edge of the lake and near the center of the lake at 110 m above sea level, respectively. Site DBB is continuously covered by water, but site DBA is covered only during the wet season in the present day. In the lake region, the average annual air temperature is 4.7°C (−14.8°C in January and 24.9°C in July) in the present day. The salinity in the lake is 347.3‰ during the dry season (May–June), and 64.3‰ during the rainy season (August–November) (Shen et al., 2001).

We collected a 15.92-m-long sediment core from site DBB in a collaboration project with Nagoya University (Japan) and Jilin University (China) in January 2004. The core was obtained by boring through the ice-covered water of the lake. We obtained no samples for analysis between 5.39 m and 15.39 m, as those core samples mainly consisted of black muddy silt and mud. Below 15 m, the DBB core consisted of white silty sand. Core sections were split, photographed, and described at the College of Earth Science, Jilin University (Changchun, China). The core sections were embedded in U-channels that were 20 cm in length and preserved by freezing. In addition, surface sediments were collected from the DBB and DBA sites by hand-powered coring on the day prior to collecting the DBB boring core. The samples were transferred to the Department of Earth and Planetary Sciences, Hokkaido University (Sapporo, Japan), for

biomarker analysis. The sediments of the DBB core were sampled from the U-channels every 2 cm in depth.

2.2. Total organic carbon (TOC) content and radiocarbon dating

Humic substances were separated from the sediments of the DBB core using 46% HF and 12 M HCl acidification, as described in Sawada (2006). The humic samples were observed under an Olympus BX41 reflected light fluorescence microscope with an Olympus ULH100HG mercury lamp, a DM400 dichroic mirror containing a 330–385-nm excitation filter, and a 420-nm-long pass barrier filter at the Department of Earth and Planetary Sciences, Hokkaido University. The light emitted was observed at 200× magnification. Radiocarbon (^{14}C) ages of the dried humic samples were determined using an accelerated mass spectrometer (AMS) at Paleolabo Co., Japan. The conventional ^{14}C ages were converted to calibrated ages by the INTCAL13 radiocarbon age calibration program. The ages of sampled horizons were derived by interpolation between radiocarbon-dated horizons.

The sediments were acidified with 4 M HCl and allowed to stand for half a day to remove carbonates. The carbonate-free samples were vacuum-dried and analyzed for TOC content using a J-Science Micro Corder JM10 at the Center for Instrumental Analysis, Hokkaido University. The precision of the TOC data in our study was ±0.2.

2.3. Lipid biomarker analysis

Extraction and separation of lipids were performed as reported in Sawada et al. (1996) and Nakamura et al. (2014). Briefly, the sediment samples were extracted with methanol (MeOH), dichloromethane (DCM)/MeOH (1/1, v/v), and DCM. As an internal standard, d_{62}-triacontane was added, and the extract was dried in a rotary evaporator and redissolved in hexane. The hexane extract was passed through a silica gel column (95%

activated), and the aliphatic and aromatic hydrocarbon fractions were eluted sequentially using hexane and hexane/toluene (3/1, v/v), then analyzed using gas chromatography–mass spectrometry (GC-MS). GC-MS was conducted using a Hewlett Packard 6890 gas chromatograph equipped with a DB-5HT column (30 m × 0.25 mm i.d. × 0.10 μm; J&W Scientific) coupled to an Agilent XL MSD quadrupole mass spectrometer (electron voltage, 70 eV; emission current, 350 μA; scan range *m/z* 50–550 in 2.91 s). The GC oven was programmed as follows: 50°C (4 min) to 300°C (held for 20 min) at 4°C/min.

The alkenones and alkenoates were quantified using gas chromatography-flame ionization detection (GC-FID) with a CP-Sil 5 CB fused silica column (50 m × 0.32 mm i.d. × 0.10 μm; Chrompack); the temperature program was as follows: 80°C (3 min) to 180°C at 10°C/min, then to 310°C (held for 15 min) at 5°C/min. Several alkenone fractions were analyzed for confirmation of precision using GC-MS and GC-FID with a VF-200ms column (60 m × 0.25 mm i.d. × 0.10 μm; Agilent) under the following GC conditions: a Shimadzu GC-2025 instrument with a VF-200ms column and a temperature program of 50°C (1 min) to 255°C at 20°C/min, then to 300°C at 3°C/min, and then to 320°C (held for 10 min) at 10°C/min. The use of the VF-200ms column was recently demonstrated by Longo et al. (2013) to significantly improve the separation of long-chain alkenones.

The *n*-alkane indicators (CPI, ACL, and *P*aq) and alkenone unsaturation indices (U^{K}_{37}, $U^{K'}_{37}$, and $U^{K''}_{37}$) were individually calculated by using conventional equations as following; CPI (Carbon preferential index): $CPI = 2([C_{25}] + [C_{27}] + [C_{29}] + [C_{31}]) / [([C_{24}] + [C_{26}] + [C_{28}] + [C_{30}]) + ([C_{26}] + [C_{28}] + [C_{30}] + [C_{32}])]$, $[C_x]$: concentrations of *n*-C_x alkanes (Bray and Evans, 1961). ACL (Average chain length): $ACL = (23[C_{23}] + 25[C_{25}] + 27[C_{27}] + 29[C_{29}] + 31[C_{31}] + 33[C_{33}]) / ([C_{23}] + [C_{25}] + [C_{27}] + [C_{29}] + [C_{31}] + [C_{33}])$ (Poynter and Eglinton, 1990; Zhang et al., 2004). *P*aq (aquatic macrophyte *n*-

alkane proxy): *P*aq = ([C_{23}] + [C_{25}]) / ([C_{23}] + [C_{25}] + [C_{29}] + [C_{31}]) (Ficken et al., 2000).

U^{K}_{37} and $U^{K'}_{37}$ were respectively calculated according to the equations of Brassell et al. (1986); U^{K}_{37} = ([37:2] - [37:4]) / ([37:2] + [37:3] + [37:4]), and Prahl and Wakeham (1987); $U^{K'}_{37}$ = [37:2] / ([37:2] + [37:3]), [x:y] : concentrations of C_x alkenones with y double bonds. Moreover, recently suggested index, $U^{K''}_{37}$, were calculated as the equation of Zheng et al. (2016); $U^{K''}_{37}$ = [37:3] / ([37:3] + [37:4]).

In addition, the chain length ratios of alkenones such as total C_{37} alkenones / total C_{38} alkenones ratio (K_{37}/K_{38}) and total C_{40} alkenones / total C_{37} alkenones ratio (K_{40}/K_{37}) as well as the percentage of $C_{37:4}$ alkenones ($\%C_{37:4}$) were respectively calculated using the following equations: K_{37}/K_{38} = ([37:2Me] + [37:3Me] + [37:4Me]) / ([38:2Et] + [38:2Me] + [38:3Et] + [38:3Me] + [38:4Et] + [38:4Me]), K_{40}/K_{37} = ([40:2Et] + [40:2Me] + [40:3Et] + [40:3Me]) / ([37:2Me] + [37:3Me] + [37:4Me]), and $\%C_{37:4}$ = [37:4Me] / ([37:2Me] + [37:3Me] + [37:4Me]) × 100.

3. Results and discussion

3.1. TOC and radiocarbon ages

TOC values in the sediments of the DBB core were nearly constant (~0.6–1.2%), although there were two decreasing spikes below the detection limit (0.3) at the 123.5-cm and 138-cm depths (Table 1, Fig. 3d). The carbon/nitrogen ratios of the DBB core (DBL1 in Tareq et al., 2006) were high (~10–30), implying that the carbon and nitrogen contents came from a mixture of sources including terrestrial plants and *in situ* aquatic production such as microalgae (Tareq et al., 2006).

The AMS ^{14}C ages were determined from humic substances (kerogens; Suppl. Figure) to be 4,832.5 ± 23.5 yr BP at the 100-cm depth and 6,348.5 ± 52.5 yr BP at the 370-cm depth, and the median probability ages were calculated to be 4,826 cal yr BP and 6,345 cal yr BP, respectively (Suppl. Table). For the reservoir effect of saline lake

water, i.e. ‘hard water’ effect, Ren (1998) reported that the radiocarbon age of sediment from lake in the arid/semiarid regions of northern China were significantly older by the hard water. Xiao et al. (2004) reported that the reservoir effect age was estimated to be ca 360 yr in the sediments from Daihai Lake in north-central China. The ^{14}C ages of the sediment samples from Dabusu Lake were possibly affected by the hard water. However, we could not determine the reservoir effect age in the lake, because the sources of organic matter used for the ^{14}C dating were likely to be not only *in situ* aquatic organism but also terrestrial plants around the lake as mentioned above. The terrestrial plants grown out of the lake might be hardly affected by the hard water. Thus, we did not correct the reservoir effect for the ^{14}C ages in our study. The sedimentary rate (SR) between these two horizons was estimated to be 0.18 cm/yr. By extrapolation using the SR, the calendar age of the lowermost layer at DBB was calculated to be 7,218 cal yr BP. It is more likely that the sediments deposited from a few hundred years ago to the present day were not recovered during coring rather than that the SR was much faster from the 100-cm depth to the surface layer. In fact, the SR estimated from the AMS ^{14}C ages (3,605 ± 135 yr BP at 320 cm and 4,605 ± 165 yr BP at 460 cm) calculated for the SNQD-2 core, which was sampled from the outer area of Dabusu Lake near the DBB core site (Fig. 1), was ~0.10 cm/yr (Jie et al., 2001; Li et al., 2001), which is similar to the SR of the DBB core.

3.2. n-*alkane proxies*

Figure 2 shows the total ion chromatogram for the apolar fraction (F1) of the sediments from the DBB core. C_{11} to C_{35} *n*-alkanes were identified in all of the study samples with the odd carbon number predominating. Maximal peaks of C_{29} and C_{31} *n*-alkanes were observed in most sediment samples, indicating that the *n*-alkanes in the DBB samples were mainly derived from leaf waxes of terrestrial vascular plants. By

contrast, C_{23} and C_{25} *n*-alkanes were dominant in some samples (75-, 123.5-, 374.5-, and 522-cm depths). The main sources of the C_{23} and C_{25} *n*-alkanes are thought to be non-emergent and submerged/floating aquatic macrophytes in lake environments (Ficken et al., 2000; Zhang et al., 2004). The *P*aq index was established as an indicator for the contribution of such aquatic macrophytes to *n*-alkane sources (Ficken et al., 2000). There were increasing spikes in the *P*aq values for the samples from the 75-, 123.5-, 374.5-, and 522-cm depths (Table 1, Fig. 3a). Nevertheless, it is presumed that aquatic macrophytes were generally a minor floral component in Dabusu Lake. The average chain length (ACL) values, including short-chain homologues (C_{23} and C_{25}; Zhang et al., 2004), were consistently constant (28.8–29.5), although the values were lower (27.97–28.35) in several layers (75-, 374.5-, and 522-cm depths) (Table 1). The ACL is an indicator of vegetation type; the leaf *n*-alkanes derived from grasslands have longer chain lengths than those from forests (Cranwell, 1973). Thus, the medium ACL values observed in our study suggest that forest/grassland mixed vegetation was generally distributed around Dabusu Lake. Lower ACL values also indicate that aquatic macrophytes had an influence on those samples, which agree with the *P*aq results.

The total *n*-alkane concentrations in the DBB samples were 0.2–18 μg/g (Table 1, Fig. 3c). The concentrations were lower in the upper parts of the DBB core, as with the trend of TOC. The carbon preferential index (CPI) values were 2.19–10.95 and were significantly lower above the 170-cm depth (Fig. 3b). The CPI represents the odd/even carbon number ratio of *n*-alkanes and has been commonly used to estimate the maturity (diagenetic level) of the sediment and the input of terrestrial plant-derived material (e.g., Brassell et al., 1986; Madureira et al., 1995). The typical *n*-alkane CPI values in vascular plant waxes are ca. 4–10 (Rieley et al., 1991). From these insights, the CPI values indicate that sediments found below the 170-cm depth commonly originate from vascular plant waxes, but the lower CPI values above the 170-cm depth indicate that

most of the *n*-alkanes found here are possibly diagenetic compounds. Also, the *n*-alkane concentrations were much lower in those layers. These results imply that fresh organic matter rarely flowed into or was deposited from the area surrounding the lake, resulting in the high contribution of compounds derived mainly from soil and weathering rock around and/or possibly far from the lake to the sediment samples.

3.3. Alkenone distribution patterns

Long-chain (C_{37}–C_{40}) di- to tetra-unsaturated alkenones were identified in all samples of the DBB core (Fig. 2). Alkenone concentrations and compositions (distribution pattern) are shown in Table 1 and Figure 3. The alkenone concentrations ranged from 0.21 to 15.44 μg/g dry sediment and tended to decrease above the 380-cm depth (Fig. 4e). The ratios of C_{37} to C_{38} alkenones (C_{37}/C_{38}) were remarkably low (0.30–0.54) in our samples (Fig. 4c). Such low C_{37}/C_{38} ratios were also reported from sediments of other Chinese continental saline lakes (Sun et al., 2004; 2007; Liu et al., 2011; Wang et al., 2015). The C_{37}/C_{38} ratios of typical marine alkenone sources, *Emiliania huxleyi* and *Gephyrocapsa oceanica*, as well as coastal and lacustrine species such as *Ruttnera lamellosa* (an updated name of the basionym *Chrysotila*; Andersen et al., 2014), are known to be lower (ca. 1–4) in cultured samples, but these are not extremely low values of <1.0 (Marlowe et al., 1984; Rontani et al., 2004; Ono et al., 2009; Nakamura et al., 2014). More recently, Araie et al. (2018) reported that the C_{37}/C_{38} ratios of the genus *Isochrysis*, especially strain Sc2, which was isolated from Canadian saline lakes, were characterized by extremely low values of <1.0 with a minimum value of 0.38. In addition, the C_{37}/C_{38} ratios are not only considered to reflect taxonomic differences but are also affected by physiological and environmental factors (Conte et al., 1998; Ono et al., 2012). Hence, the low K_{37}/K_{38} ratios observed in our study and in studies of other Chinese inland lakes might also be attributable to specific

but unrelated physiological and environmental factors to some extent. In the sediments from Dabusu Lake, C_{38} ethyl ketones were dominant, but C_{38} methyl ketones were hardly detected. Also, significant amounts of C_{40} alkenones were detected in all samples, and the C_{40}/C_{37} alkenone ratios were noticeably high (0.08–0.22; Fig. 4b). Tetra-unsaturated alkenones were also abundantly detected, and the percentages of $C_{37:4}$ alkenones among total alkenones (%$C_{37:4}$) ranged from 15.3% to 38.3% (Fig. 4d). These values are characteristics of Group II alkenone producers (Isochrysidaceae including *Ruttnera* and *Isochrysis*) as suggested by Theroux et al. (2010), especially, *R. lamellosa* and *Isochrysis* sp. (strain Sc2). The C_{40}/C_{37} ratios of *Isochrysis* were found to be lower (0.01–0.15; Araie et al., 2018). Thus, we presume that *R. lamellosa* rather than *Isochrysis* might be the main alkenone producer in Dabusu Lake. However, haptophyte rDNA analysis will be necessary to determine the species of the alkenone producers.

3.4. Alkenone-based paleotemperature

The values of alkenone unsaturation indices (U^{K}_{37}, $U^{K'}_{37}$, and $U^{K''}_{37}$) varied by depth in the DBB core (Table 1, Fig. 4a). We estimated water temperatures from U^{K}_{37} using the U^{K}_{37}-temperature (T) calibration obtained from culture strain *R. lamellosa* CCMP1307 (Nakamura et al., 2014) as follows: $U^{K}_{37} = 0.045\ T - 1.016$. *Ruttnera lamellosa* was estimated to be the most appropriate alkenone producer from the alkenone fingerprints. These water temperatures ranged from 17.2 to 23.6°C (Table 1, Fig. 5a), which are ca. 1–6°C lower than the mean air temperature in summer (July) (MATS; 24.9°C) around Dabusu Lake in the present day. On the other hand, using the U^{K}_{37}-T calibration with *Isochrysis* strain Sc2 (Araie et al., 2018; $U^{K}_{37} = 0.039\ T - 0.70$), the water temperatures were estimated to be 11.0–17.7°C (Table 1, Fig. 5a). The variation patterns of T calculated using the U^{K}_{37}-T equations are similar between strains CCMP1307 and Sc2, because the slopes in these equations are almost the same.

Noticeable increasing spikes of the U^{K}_{37}-based water temperatures were observed at ca. 7.2 kyr BP, 6.2–6.0 kyr BP, and 5.5–5.3 kyr BP in the DBB core.

Recently, Zheng et al. (2016) proposed that $U^{K''}_{37}$, in which only $C_{37:3}$ and $C_{37:4}$ alkenones are used and $C_{37:2}$ homologues are omitted, serves as a better thermometer for the Group II alkenone producers, which tightly control the abundance of tetra-unsaturated alkenones (i.e., $C_{37:4}$) in response to temperature changes. Indeed, considerably higher coefficients were observed for the $U^{K''}_{37}$-T linear regression than for $U^{K'}_{37}$-T and $U^{K'}_{38}$-T in both cultured and environmental samples investigated in their study. They demonstrated that the $C_{37:4}$ alkenone is more responsible for the temperature-regulated response in the alkenone composition than $C_{37:2}$. Therefore, we applied the $U^{K''}_{37}$-T calibration obtained from culture strain *R. lamellosa* strain LG (Zheng et al., 2016) to calculate temperatures in the Dabusu samples, using the following equation: $U^{K''}_{37} = 0.042\ T - 0.08$. These water temperatures ranged from 14.6 to 21.1°C (Table 1, Fig. 5a). These temperature ranges are ca. 3–10°C lower than the present MATS (24.9°C) around Dabusu Lake. The variation pattern of the $U^{K''}_{37}$-based water temperatures is almost similar to that of the U^{K}_{37}-based water temperatures. However, a rapid decreasing spike in the $U^{K''}_{37}$-based water temperatures was observed at ca. 6.2 kyr in the DBB core, whereas the U^{K}_{37}-based summer water temperatures rapidly increased at that time. Basically, $U^{K''}_{37}$-based water temperatures were ~2°C lower than U^{K}_{37}-based (CCMP1307) water temperatures.

Summer water temperatures based on $U^{K'}_{37}$ were calculated using the following equation established from the mean surface water temperatures in July of several Chinese lakes (Chu et al., 2005): $U^{K'}_{37} = 0.033\ T - 0.367$. The summer temperatures were estimated to range from 16.0 to 20.8°C in the DBB core (Table 1, Fig. 5b), which is ca. 5–9°C lower than the present MATS around Dabusu Lake. The $\%C_{37:4}$ values were clearly lower in the samples represented by increasing spikes of U^{K}_{37}-based water

temperatures, indicating that the change in estimated temperatures was linked to declines in tetra-unsaturated alkenones. The $C_{37:4}$ alkenone may respond more directly to temperature conditions than $C_{37:2}$ as mentioned above, and thus the $U^{K'}_{37}$ index calculated without $C_{37:4}$ is thought to be less reliable as a thermometer for sediment samples from inland saline lakes such as Dabusu Lake, which is inhabited by Group II haptophytes.

3.5. Reconstruction of paleoclimatic variations in northeastern China

Figure 6 shows the variations in the alkenone-based temperatures and paleovegetation reconstructed using terrestrial plant-derived biomarkers in the DBB samples. The $U^{K''}_{37}$-based water temperatures were roughly estimated to be lower (ca. 16°C) from 7.2 to 6.2 kyr BP, although a higher peak was observed at ca. 7.2 kyr BP. These temperatures rapidly decreased at ca. 6.2 kyr BP, and subsequently increased (ca. 15–21°C) after 6.2 kyr BP. This general trend of the alkenone-based temperatures is concordant with those of paleoclimatic variations in Dabusu Lake as reported previously. According to Shen et al.(2004), the geochemical records such as carbonate content and $\delta^{13}C$ of organic matter in sediments from the site Xuezijing of Dabusu Lake (Fig. 1B) suggested that the climate was cool and humid in ca. 7.8–6.7 kyr BP, and subsequently reached a relatively stable warm and arid stage after ca. 6.7 kyr BP. Also, the grain size and carbonate contents of sediments from the site of SNQD-2 of Dabusu Lake (Fig. 1B) indicated that the lake level was high attributed to the warm-humid climate during 5.4–3.6 kyr BP and declined after 3.6 kyr BP (Jie et al., 2001). Noticeably, the alkenone-based temperatures were estimated to have peaked (ca. 20–21°C) from 5.5 to 5.3 kyr BP, indicating that this maximal stage was the Holocene Thermal Maximum (HTM) in the Dabusu region. Xiao et al. (2004) suggested that the Holocene Optimum was observed in the north-central China region from ca. 7.9 to 4.5 kyr BP, and maximal peaks of

temperature and precipitation were observed from 6.05 to 5.1 kyr BP, during the climatic maximum (the HTM). In addition, Cui et al. (2009) demonstrated that palynological data indicated the mid-Holocene warm-humid phases in the North China Plain during ca. 5.0–3.0 kyr BP., which is 1-2 kyrs younger ages compared with our alkenone records. Zhao and Yu (2012) synthesized time-series data for vegetation and climate using pollen analysis for the monsoonal margin region of China demonstrated that the general climatic variation pattern in the margin region was slightly humid in the early Holocene, mostly arid in the middle Holocene, and arid in the late Holocene, although there was regional variability, as reflected by vegetation change.

The markedly decreasing spikes of $U^{K"}_{37}$-based water temperatures in our study likely corresponded to the cooling events during the Holocene Optimum, as suggested in previous reports (Bond et al., 2001; Dykoski et al., 2005; Wang et al., 2005; Li et al., 2011). In particular, the rapid decreasing spike in our temperature data at 6.2 kyr BP based on stalagmite $\delta^{18}O$ values was possibly associated with the cooling regime just after Asian monsoon event (AM) 1, as reported by Wang et al. (2005). Also, the increasing spike in our temperature data at 7.2 kyr BP may reflect the recorded rapid warming regime observed just after AM2. These AMs are thought to be local cooling events that were possibly related to weak monsoon climatic settings observed in southern China and their detection could be evidence for the climatic influence of these events even in northeastern China in our study. Moreover, the decreasing of our temperature data during 5.6 kyr BP may be associated with the cooling of Bond event 4 (BE4; 5.6–5.5 kyr BP) as shown in Wang et al. (2005), although the increasing spike of stalagmite $\delta^{18}O$ values was unclear during the BE4. Just after the BE4, the increasing trends of the alkenone-based temperatures seemed to be synchronous to those of stalagmite $\delta^{18}O$ values. Li et al. (2011) demonstrated that the pollen records from Jingbo Lake (northeastern China) showed a weakened summer monsoon during 5.7–5.4 kyr BP,

coinciding with the abrupt cooling events recorded in the $\delta^{18}O$ values of the Dongge cave (Dykoski et al., 2005; Wang et al., 2005) rather than a gradual decline in monsoon intensity through the Holocene. However, the time resolution of the age model in our study was rough to discuss these centennial time-scale climatic events, so that more precise investigation is needed in future.

At ca. 6.2 kyr BP, the baseline of the reconstructed water temperatures became 1–2°C warmer synchronously with paleovegetation changes as reconstructed via lignin analysis (Tareq et al., 2006). The syringaldehyde/vanillin ratios in the lignin rapidly decreased at 6.2 kyr BP, indicating that herbaceous angiosperm-dominant vegetation was rapidly replaced by woody gymnosperm-dominant vegetation. This trend in vegetation variation is concordant with that estimated by a pollen study of Daihai Lake in north-central China (Xiao et al., 2004).

Variations in the relative abundances of aquatic macrophytes as estimated using the *P*aq index of *n*-alkanes were hardly synchronous to those estimated using lignin and alkenone-based temperatures. However, the rapidly increasing spikes of the *P*aq index corresponded to those of alkenone-based temperatures at 7.2 kyr BP (just after AM2) and 6.4 kyr BP (Fig. 6). These increasing spikes in *P*aq values can be interpreted to indicate that aquatic macrophytes flourished within/around Dabusu Lake due to more humid conditions, which increased the level of the lake water under high precipitation. Moreover, the aquatic macrophytes possibly flourished by high nutrition in the lake environment resulting from the expansion of the lake water under humid condition. The rapid warming reconstructed by the alkenone-based temperatures might have resulted in increased precipitation around the lake at those ages, especially just after the AM2 cooling event. In addition, *P*aq values tended to increase from ca. 5 to 4.5 kyr BP, indicating that the aquatic macrophytes mostly flourished within/around Dabusu Lake as a result of increased precipitation under warm conditions. However, the timing of the

*P*aq maximum was clearly different from the HTM reconstructed using alkenone-based temperatures. These results suggest that climatic signals are different between air/water temperature and precipitation in the intercontinental lake region.

Our alkenone record of Dabusu Lake sediments shows a slight general increasing trend after ca. 7.2 kyr BP (Fig. 6), but the $\delta^{18}O$ values of the Dongge cave in southern China suggest gradually weakened the East Asian monsoon after 7.2 kyr BP (Dykoski et al., 2005; Wang et al., 2005). The different trends may be explained by the different climatic influences against the East Asian summer monsoon between northern and southern China regions. Dabusu Lake is located at a confluence zone of the East Asian summer and winter monsoons, and therefore, the lake region is affected by both monsoons (Fig. 1A). However, the lacustrine alkenones were thought to be mainly produced in warm seasons such as spring to fall based on the data from the lake in North America (Toney et al., 2010), although the seasonality of alkenone production in lake environments has been unclear. Moreover, the alkenone producer(s) could not grow in winter of the northern China lakes such as Dabusu Lake due to freezing of lake water. Thus, the alkenone-based temperatures likely reflected the climatic variations in only warm seasons, affected by the summer monsoon. The East Asia summer monsoon, basically an onshore flow of warm and moist air masses from low latitudes of the Pacific, varies depending on globally the variations of solar insolation and locally oceanic settings of the western Pacific. Particularly, the Kuroshio current, which is the strong northwestern component of the North Pacific subtropical circulation, is an important ocean current system for the heat transport from low to middle latitudinal areas of the East Asia, and is thought to be closely associated with the variations in the East Asia summer monsoon. It was reported that the Kuroshio current was presumably intensified at 8–7 kyr BP, and was weaken after 7 kyr BP during mid-Holocene (Sawada and Handa, 1998; Sagawa et al., 2011). Indeed, the variations in the sea surface

temperatures related to the Kuroshio intensity were synchronous with those of the $\delta^{18}O$ of the Dongge cave in southern China (Yuan et al., 2004; Sagawa et al., 2011). However, the Kuroshio hardly have a direct influence to the northern East Asia regions such as the northern China. From these insights, we infer that the temperatures of warm seasons in northern Chinese regions such as the Dabusu Lake had a less influence by the East Asian summer monsoon associated with the oceanographic variations in the western Pacific. Thus, the general trend in our temperature record of Dabusu Lake during the Holocene Optimum is different from those in the typical East Asian summer monsoon regions including the southern China, but is concordant with those of vegetation records in northern Chinese regions (Xiao et al., 2004).

4. Conclusions

We analyzed long-chain *n*-alkanes and alkenones in sediments from Dabusu Lake in northeastern China from ca. 7.2 to 4.5 kyr BP (the Holocene Optimum) and the present. Long-chain *n*-alkanes are derived from leaf waxes of terrestrial vascular plants and aquatic macrophytes. Using *n*-alkane proxies such as the *P*aq and ACL indices, variations in paleovegetation were reconstructed. Although there were several increasing spikes, *P*aq values were generally low, indicating that aquatic macrophytes were minor floral components in Dabusu Lake. The ACL data indicate that forest/grassland mixed vegetation was generally distributed around the lake.

The alkenone distribution patterns of markedly low C_{37}/C_{38}, high C_{40}/C_{37}, and high $\%C_{37:4}$ ratios in the Dabusu samples suggest that the main alkenone producers were the Group II producers, especially *R. lamellosa*. We estimated water temperatures based on alkenone unsaturation indices (U^{K}_{37} and $U^{K"}_{37}$) using the temperature calibrations obtained from culture strains of *R. lamellosa*. The variation pattern of the $U^{K"}_{37}$-based water temperatures was almost similar to that of U^{K}_{37}-based water

temperatures, and generally, the $U^{K"}_{37}$-based temperatures were ~2°C lower than U^{K}_{37}-based temperatures. However, the calculated spikes in water temperatures differed when U^{K}_{37}- and $U^{K"}_{37}$-based calibrations were used.

The $U^{K"}_{37}$-based water temperatures were roughly estimated to be lower (ca. 16°C) from 7.2 to 6.2 kyr BP, although a higher peak was observed at 7.2 kyr BP. These temperatures rapidly decreased at ca. 6.2 kyr BP, and then subsequently increased (ca. 15–21°C). Alkenone-based temperatures peaked from 5.5 to 5.3 kyr BP in our study, indicating that this maximal stage is the HTM in the Dabusu region. The markedly decreasing spikes of $U^{K"}_{37}$-based water temperatures in our study likely corresponded to the cooling events such as the AM1 (6.2 kyr BP) and BE4 (5.6–5.5 kyr BP) during the Holocene Optimum. Also, the increasing (7.2 kyr BP) spikes in temperature based on stalagmite $\delta^{18}O$ values were possibly associated with the warming regimes just after AM2. Moreover, the rapidly increasing spikes of alkenone-based temperatures corresponded to those of *P*aq values at 7.2 kyr BP (just after AM2) and 6.4 kyr BP. These results imply that the rapid warming reconstructed using alkenone-based temperatures might have resulted in increased precipitation around the lake at those ages, especially just after the AM2 cooling event. In addition, the increasing trends of alkenone-based water temperatures were similar to those of paleovegetation changes reconstructed using lignin ratios, as reported previously. The combined records of multiple biomarkers, including long-chain *n*-alkanes and alkenones, as well as lignin, provide a robust means of reconstructing climatic pulses in intercontinental lake regions.

Acknowledgements

We are very grateful to (the late) Prof. N. Handa of Nagoya University for designing, promoting and summarizing the Dabusu project. We thank Prof. Hu Ke of Jilin University, China (present: China University of Geosciences), Drs. B. Chen, D. Jie and

X. Zhang of Jilin University as well as Drs. N. Inouye and M. Fukuoka of Nagoya University for help in the field works and core sampling, and Prof. H. Kitagawa of Nagoya University for valuable discussion. We also thank Miss Y. Hattori for help in analysis. We are grateful to two anonymous reviewers for constructive comments. The study was supported in part by JSPS KAKENHI Grant Numbers 14209012 (to N.H.), 26287130 (to K.S.) and 18H01322 (to K.S.).

References

Andersen, R.A., Kim, J.I., Tittley, I., Yoon, H.S., 2014. A re-investigation of *Chrysotila* (Prymnesiophyceae) using material collected from the type locality. Phycologia 53, 463–473.

Araie, H., Nakamura, H., Toney, J.L., Haig, H.A., Plancq, J., Shiratori, T., Leavitt, P.R., Seki, O., Ishida, K., Sawada, K., Suzuki, I., Shiraiwa, Y., 2018. Novel alkenone-producing strains of genus *Isochrysis* (Haptophyta) isolated from Canadian saline lakes show temperature sensitivity of alkenones and alkenoates. Org. Geochem. 121, 89–103.

Brassell, S.C., Eglinton, G., Marlowe, I.T., Pflaumann, U., Sarnthein, M., 1986. Molecular stratigraphy: a new tool for climatic assessment. Nature 320, 129–133.

Bond, G., Kromer, B., Beer, J., Muscheler, R., Evans, M.N., Showers, W., Hoffmann, S., Lotti-Bond, R., Hajdas, I., Bonani, G., 2001. Persistent solar influence on North Atlantic climate during the Holocene. Science 294, 2130–2136.

Boot, C.S., Ettwein, V.J., Maslin, M.A., Weyhenmeyer, C.E., Pancost, R.D., 2006. 35,000 year record of terrigenous and marine lipids in Amazon Fan sediments. Org. Geochem. 37, 208–219.

Brassell, S.C., Brereton, R.G., Eglinton, G., Grimalt, J., Liebezeit, G., Marlowe, I.T., Pflaumann, U., Sarnthein, M., 1986. Palaeoclimatic signals recognized by chemometric treatment of molecular stratigraphic data. Org. Geochem. 10, 661–669.

Bray, E.E., Evans, E.D., 1961. Distributions of *n*-parafins as a clue to the recognition of source beds. Geochim. Cosmochim. Acta 27, 1113–1127.

Conte, M.H., Thompson, A., Lesley, D., Harris, R.P., 1998. Genetic and physiological influences on the alkenone/alkenoate versus growth temperature relationship in

Emiliania huxleyi and *Gephyrocapsa oceanica*. Geochim. Cosmochim. Acta 62, 51–68.

Cranwell, P.A., 1973. Chain-length distribution of *n*-alkanes from lake sediments in relation to post-glacial environmental change. Freshwater Biology 3, 259–265.

Cui, J., Zhou S., Chang, H., 2009. The Holocene warm-humid phases in the North China Plain as recorded by multi-proxy records. Chin. J. Oceanol. Limnol. 27, 147–161.

Dykoski, C.A., Edwards, R.L., Chen, H., Yuan, D.X., Cai, Y.J., Zhang, M.L., Lin, Y.S., Qing, J.M., An, Z.S., Revenaugh, J., 2005. A high-resolution absolute-dated Holocene and deglacial Asian monsoon record from Dongge cave, China. Earth Planet. Sci. Lett. 233, 71–86.

Fisher, E., Oldfield, F., Wake, R., Boyle, J., Appleby, P., Wolff, G.A., 2003. Molecular marker records of land use change. Org. Geochem. 34, 105–119.

Ficken, K.J., Li, B., Swain, D.L., Eglinton, G., 2000. An *n*-alkane proxy for the sedimentary input of submerged/floating aquatic macrophytes. Org. Geochem. 31, 745–749

Jie, D., Lu, J., Li, Z., Leng X., Wang S., Zahng G., 2001. Carbonate content of sedimentary core and Holocene lake-level fluctuation of Dabusu lake. Mar. Geol. Quat. Geol. 21, 77–82. (in Chinese).

Li, Z., Lu, J., 2001. Geomorphology, deposition and lake evolution of Dabusu Lake, northeastern China. J. Lake Sci. 13, 103–110. (in Chinese).

Li, C., Wu, Y., Hou, X., 2011. Holocene vegetation and climate in Northeast China revealed from Jingbo Lake sediment. Quat. Int. 229, 67-73.

Li, Y., Yang, S., Wang, X., Hu, J., Cui, L., Huang, X., Jiang, W., 2016. Leaf wax *n*-alkane distributions in Chinese loess since the Last Glacial Maximum and implications for paleoclimate. Quat. Int. 399, 190e197.

Liu, W., Liu, Z., Wang, H., He, Y., Wang, Z., Xu, L., 2011. Salinity control on long-chain alkenone distributions in lake surface waters and sediments of the northern Qinghai-Tibetan Plateau, China. Geochim. Cosmochim. Acta 75, 1693–1703.

Liu, Z., Henderson, A.C.G., Huang, Y., 2006. Alkenone-based reconstruction of late-Holocene surface temperature and salinity changes in Lake Qinghai, China. Geophys. Res. Lett. 33, L09707. doi:10.1029/2006GL026151.

Longo, W. M., Dillon, J. T., Tarozo, R., Salacup, J. M., Huang, Y., 2013. Unprecedented separation of long chain alkenones from gas chromatography with a poly(trifluoropropylmethylsiloxane) stationary phase. Org. Geochem. 65, 94–102.

Madureira, L.A.S., Conte, M.H., Eglinton, G., 1995. Early diagenesis of lipid biomarker compounds in North Atlantic sediments. Paleoceanography 10, 627–642.

Marlowe, I., Brassell, S., Eglinton, G., Green, J., 1984. Long chain unsaturated ketones and esters in living algae and marine sediments. Org. Geochem. 6, 135–141.

Nakamura, H., Sawada, K., Araie, H., Suzuki, I., Shiraiwa, Y., 2014. Long chain alkenes, alkenones and alkenoates produced by the haptophyte alga *Chrysotila lamellosa* CCMP1307 isolated from a salt marsh. Org. Geochem. 66, 90–97.

Ono, M., Sawada, K., Shiraiwa, Y., Kubota, M., 2012. Changes in alkenone and alkenoate distributions during acclimatization to salinity change in *Isochrysis galbana*: Implication for alkenone-based paleosalinity and paleothermometry. Geochem. J. 46, 235–247.

Ono, M., Sawada, K., Kubota, M., Shiraiwa, Y., 2009. Change of the unsaturation degree of alkenone and alkenoate during acclimation to salinity change in *Emiliania huxleyi* and *Gephyrocapsa oceanica* with reference to a palaeosalinity indicator. Res. Org. Geochem. 25, 53–60.

Poynter, J., Eglinton, G., 1990. Molecular composition of three sediments from hole 717C: The Bengal Fan, edited by J. R. Cochran et al., Proceedings of Ocean Drilling Program, Scientific Results, 116, 155–161.

Prahl, F.G., Wakeham, S.G., 1987. Calibration unsaturation patterns in long-chain ketone composition for paleotemperature assessment. Nature 330, 367–369.

Prahl, F.G., Muehlhausen, L.A., Zahnle, D., 1988. Further evaluation of long-chain alkenones as indicators of paleoceanographic condition. Geochim. Cosmochim. Acta 52, 2303–2310.

Randlett, M.-E., Coolen, M.J.L., Stockhecke, M., Pickarski, N., Litt, T., Balkema, C., Kwiecien, O., Tomonaga, Y., Wehrli, B., Schubert, C.J., 2014. Alkenone distribution in Lake Van sediment over the last 270 ka: influence of temperature and haptophyte species composition. Quat. Sci. Rev. 104, 53e62.

Regnery, J., Püttmann, W., Koutsodendris, A., Mulch, A., Pross, J., 2013. Comparison of the paleoclimatic significance of higher land plant biomarker concentrations and

pollen data: A case study of lake sediments from the Holsteinian interglacial. Org. Geochem. 61, 73–84.

Ren, G., 1998. A finding of the influence of ‘‘hard water’’ on radiocarbon dating for lake sediments in Inner Mongolia, China. Jour Lake Sci 10, 80–82 (in Chinese).

Rieley, G., Collier, R.J., Jones, D.M., Eglinton, G., 1991. The biogeochemistry of Ellesmere Lake, UK, I, Source correlation of leaf wax inputs to the sedimentary lipid record. Org. Geochem. 17, 901–912.

Rontani, J.-F., Beker, B., Volkman, J.K., 2004. Long-chain alkenones and related compounds in the benthic haptophyte Chrysotila lamellosa Anand HAP 17. Phytochemistry 65, 117–126.

Sagawa, T., Yokoyama, Y., Ikehara, M., Kuwae, M., 2011. Vertical thermal structure history in the western subtropical North Pacific since the Last Glacial Maximum. Geophys. Res. Lett. 38, L00F02. doi:10.1029/2010GL045827

Sawada, K., 2006. Organic facies wand geochemical aspects in Neogene neritic sediments of the Takafu syncline area of central Japan: Paleoenviromental and sedimentological reconstructions. Isl. Arc 15, 517–536.

Sawada, K., Handa, N., 1998. Variability of the path of the Kuroshio ocean current over the past 25,000 years. Nature 392, 592–595.

Sawada, K., Handa, N., Shiraiwa, Y., Danbara, A., Montani, S., 1996. Long-chain alkenones and alkyl alkenoates in the coastal and pelagic sediments of the northwest North Pacific, with special reference to the reconstruction of *Emiliania huxleyi* and *Gephyrocapsa oceanica* ratios. Org. Geochem. 24, 751–764.

Sun, Q., Chu, G., Liu, G., Li, S., Wang, X., 2007. Calibration of alkenone unsaturation index with growth temperature for a lacustrine species, *Chrysotila lamellosa* (Haptophyceae). Org. Geochem. 38, 1226–1234.

Sun, Q., Chu, G., Li, S., Lü, C., Zheng M., 2004. Long-chain alkenones in sulfate lakes and its paleoclimatic implications. Chin. Sci. Bull. 49, 2082–2086.

Shen, J., Zhang, E., Yang, X., Matsumoto, R., 2004. Paleoclimatic changes inferred from carbon isotope composition of organic matter in sediments of Dabusu Lake, Jilin Province, China. Chin. J. Oceanol. Limnol. 22, 124–129.

Tareq, S.M., Handa, N., Tanoue, E., 2006. A lignin phenol proxy record of mid Holocene paleovegetation changes at Lake DaBuSu, northeast China. J. Geochem.

Explor. 88, 445–449.

Theroux, S., D'Andrea, W.J., Toney, J., Amaral-Zettler, L., Huang, Y., 2010. Phylogenetic diversity and evolutionary relatedness of alkenone-producing haptophyte algae in lakes: implications for continental paleotemperature reconstructions. Earth Planet. Sci. Lett. 300, 311–320.

Toney J. L., Huang Y., Fritz S. C., Baker P. A., Grimm E. and Nyren P. (2010) Climatic and environmental controls on the occurrence and distribution of long chain alkenones in lakes. Geochim. Cosmochim. Acta 74, 1563–1578.

Wang, Y., Cheng, H., Edwards, R.L., He, Y., Kong, X., An, Z., Wu, J., Kelly, M.J., Dykoski, C.A., Li, X., 2005. The Holocene Asian monsoon: Links to solar changes and North Atlantic climate. Science 308, 854–857.

Wang, Z., Liu, Z., Zhang, F., Fu, M., An, Z., 2015. A new approach for reconstructing Holocene temperatures from a multi-species long chain alkenone record from Lake Qinghai on the northeastern Tibetan Plateau. Org. Geochem. 88, 50–58.

Xiao, J., Xu, Q., Nakamura, T., Yang, X., Liang, W., Inouchi, Y., 2004. Holocene vegetation variation in the Daihai Lake region of north-central China: a direct indication of the Asian monsoon climatic history. Quat. Sci. Rev. 23, 1669–1679.

Yuan, D., Cheng, H., Edwards, R. L., Dykoski, C. A., Kelly, M. J., Zhang, M., Qing, J., Lin, Y., Wang, Y., Wu, J., Dorale, J. A., An, Z., Cai, Y., 2004. Timing, duration, and transitions of the last interglacial Asian monsoon, Science, 304, 575–578.

Zhang, J.C., Lin, Z.G., 1992. Climate of China. Wiley, New York, 376pp.

Zhang, Z., Zhao, M., Yang, X., Wang, S., Jiang, X., Oldfield, F., Eglinton, G., 2004. A hydrocarbon biomarker record for the last 40 kyr of plant input to Lake Heqing, southwestern China. Org. Geochem. 35, 595–613.

Zheng, Y., Huang, Y., Andersen, R.A., Amaral-Zettler, L.A., 2016. Excluding the diunsaturated alkenone in the U^{K}_{37} index strengthens temperature correlation for the common lacustrine and brackish-water haptophytes. Geochim. Cosmochim. Acta 175, 36–46.

Zhao, Y., Yu, Z., 2012. Vegetation response to Holocene climate change in East Asian monsoon-margin region. Earth-Sci. Rev. 113, 1–10.

Captions

Table 1 Data of total organic carbon content (TOC; %), concentrations of total *n*-alkanes and long chain alkenones (μg/g dry sediment) and the ratios of these compounds against TOC, *n*-alkane indicators such as carbon preferential index (CPI), average chain length (ACL), and aquatic plant *n*-alkane proxy (*P*aq) as well as alkenone proxies such as alkenone unsaturation indices (U^{K}_{37} and $U^{K'}_{37}$), the percentage of $C_{37:4}$ alkenones ($\%C_{37:4}$), chain length ratio of alkenones (C_{37}/C_{38} and C_{40}/C_{37}), as well as alkenone-based temperatures. $U^{K'}_{37}$-based summer (July) lake surface water temperatures calculated by the equations reported by Chu et al. (2005) (*1), U^{K}_{37}-based water temperatures by the equations reported by Nakamura et al. (2012) (*2) and Araie et al. (2018) (*3), and $U^{K''}_{37}$-based water temperatures by the equations reported by Zhang et al. (2016) (*4). (See text).

Figure 1 (A) Map showing the locations of Lake Dabusu in the northeastern China. Climatic regimes are also shown. A bold dashed line and arrows are the average landward limit of summer monsoonal front of the present July, and dominant wind vectors, respectively. The winter monsoon winds associated with the Siberian–Mongolian High is also shown. After Zhang and Lin (1992), and Xiao et al. (2004). (B) Sites of DBB cores. The sites of cores collected previously are also shown; 1: site Xuezijing (Shen et al., 2001), 2: site of SNQD-2 core (Jie et al., 2001; Li et al., 2001). Geomorphic distribution- a: present swamp wetland, b: lake water area, c: terrace with elevation of 122 m - 124 m.

Figure 2 (a) Total ion chromatogram (TIC) of apolar fraction F1, and gas chromatograms of mid-polar fraction F3 measured with a CPSil 5CB column (b) and with a VF-200 ms column (c) of a sediment in DBB 10-4 (522 cm depth). Numbers

in TIC are *n*-alkanes (carbon numbers). Peaks of x:yMe or Et are x carbon number methyl (Me) or ethyl (Et) alkenones with y double bonds (e.g. 37:3Me: C_{37} tri-unsaturated methyl alkenone). Peaks a-d: unidentified compounds.

Figure 3 Depth profiles of the values of *n*-alkane proxies such as (a) aquatic macrophyte index (*P*aq) and (b) carbon preferential index (CPI), (c) total *n*-alkane concentrations, and (d) TOC in DBB samples of Dabusu Lake. Calendar ages are also shown.

Figure 4 Depth profiles of (a) alkenone unsaturation indices (U^{K}_{37}, $U^{K'}_{37}$, and $U^{K''}_{37}$), chain length ratio of alkenones ((b) C_{40}/C_{37}, (c) C_{37}/C_{38}), (d) the percentage of $C_{37:4}$ alkenones ($\%C_{37:4}$), and (e) total alkenone concentrations. Calendar ages are also shown.

Figure 5 Age profiles of (a) variations in U^{K}_{37}-based water temperatures estimated using the calibrations obtained from *R. lamellosa* CCMP1307 (U^{K}_{37} = 0.045 T – 1.016; Nakamura et al., 2014) and *Isochrysis* Sc2 (Araie et al., 2018; U^{K}_{37} = 0.039 T – 0.70), as well as $U^{K''}_{37}$-based water temperatures estimated using the calibrations from *R. lamellosa* LG strain (U^{K}_{37} = 0.042 T – 0.08; Zhang et al., 2016), and (b) $U^{K'}_{37}$-based summer water temperatures calculated using the calibration of $U^{K'}_{37}$ of lacustrine sediments against the water temperatures of July in several Chinese lakes ($U^{K'}_{37}$ = 0.033 T – 0.367; Chu et al., 2005).

Figure 6 (a) Oxygen isotope ratio ($\delta^{18}O$) records in stalagmite of the Dongge Cave, southern China (Wang et al., 2005). AM 1 and AM 2 indicate Asian Monsoon events (Wang et al., 2005) and BE4 indicates Bond Event 4 (Bond et al., 2001). (b) Variations in $U^{K''}_{37}$-based water temperatures estimated using the calibration

obtained from *R. lamellosa* LG strain ($U^{K''}_{37}$ = 0.045 T – 1.016; Zheng et al., 2014) in the DBB samples of Dabusu Lake. Paleovegetation records of a DBB core of Dabusu Lake; (c) variations in angiosperm / gymnosperm ratios estimated by the lignin ratios such as syringyl / vanillyl (S/V) and cinnamyl / vanillyl (C/V) ratios (Tareq et al., 2006), and (d) relative abundances of aquatic macrophytes estimated by *P*aq values in the DBB samples of Dabusu Lake.

Supplementary data 1 Radiocarbon (^{14}C) ages of a DBB core in Lake Dabusu.

Supplementary figure Microphotographs by transmitted (left) and fluorescent (right) light microscopic observations of humic substances (kerogen-like matter) from the sediments at 100-cm and 370-cm depths in Lake Dabusu. FA: fluorescent amorphous organic matter, NFA: non-fluorescent amorphous organic matter, WFA: weakly-fluorescent amorphous organic matter, spo: sporomorph, sub: suberin, wood: wood fragment.

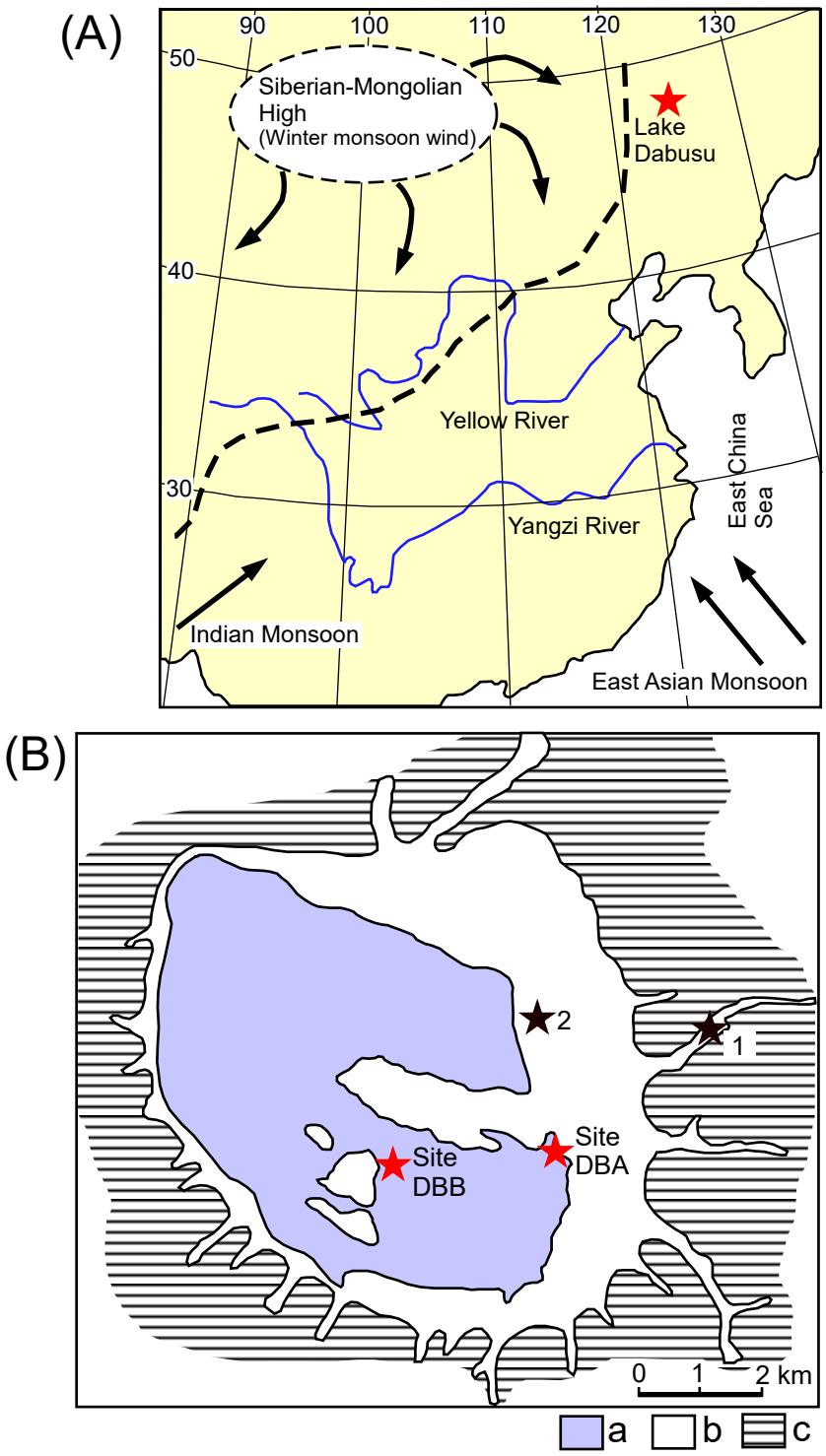

Figure 1 (A) Map showing the locations of Lake Dabusu in the northeastern China. Climatic regimes are also shown. A bold dashed line and arrows are the average landward limit of summer monsoonal front of the present July, and dominant wind vectors, respectively. The winter monsoon winds associated with the Siberian-Mongolian High is also shown. After Zhang and Lin (1992), and Xiao et al. (2004). (B) Sites of DBB cores. The sites of cores collected previously are also shown; 1: site Xuezijing (Shen et al., 2001), 2: site of SNQD-2 core (Jie et al., 2001; Li et al., 2001). Geomorphic distribution- a: present swamp wetland, b: lake water area, c: terrace with elevation of 122 m - 124 m.

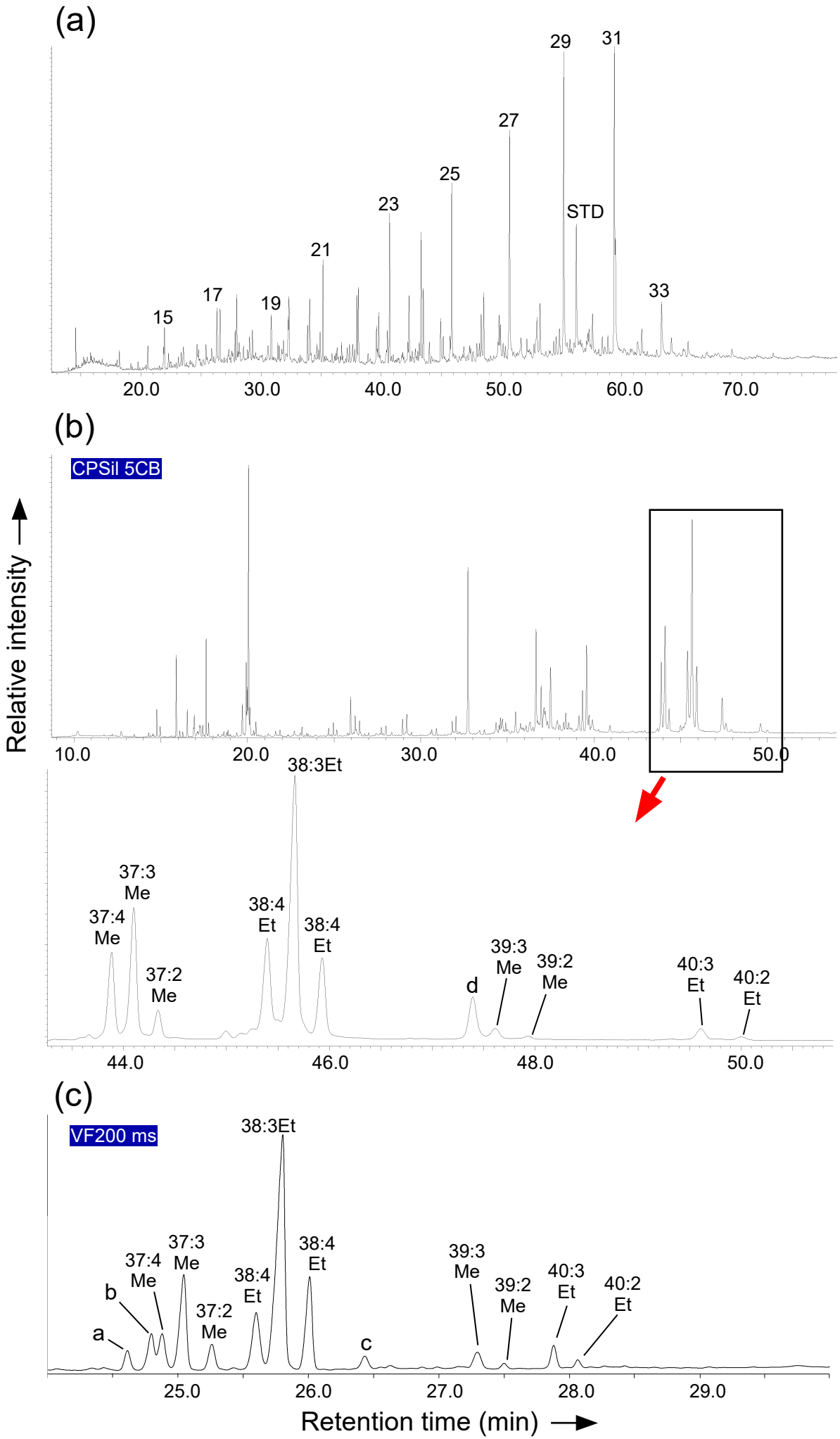

Figure 2 (a) Total ion chromatogram (TIC) of apolar fraction F1, and gas chromatograms of mid-polar fraction F3 measured with a CPSil 5CB column (b) and with a VF-200 ms column (c) of a sediment in DBB 10-4 (522 cm depth). Numbers in TIC are *n*-alkanes (carbon numbers). Peaks of x:yMe or Et are x carbon number methyl (Me) or ethyl (Et) alkenones with y double bonds (e.g. 37:3Me: C_{37} tri-unsaturated methyl alkenone). Peaks a-d: unidentified compounds.

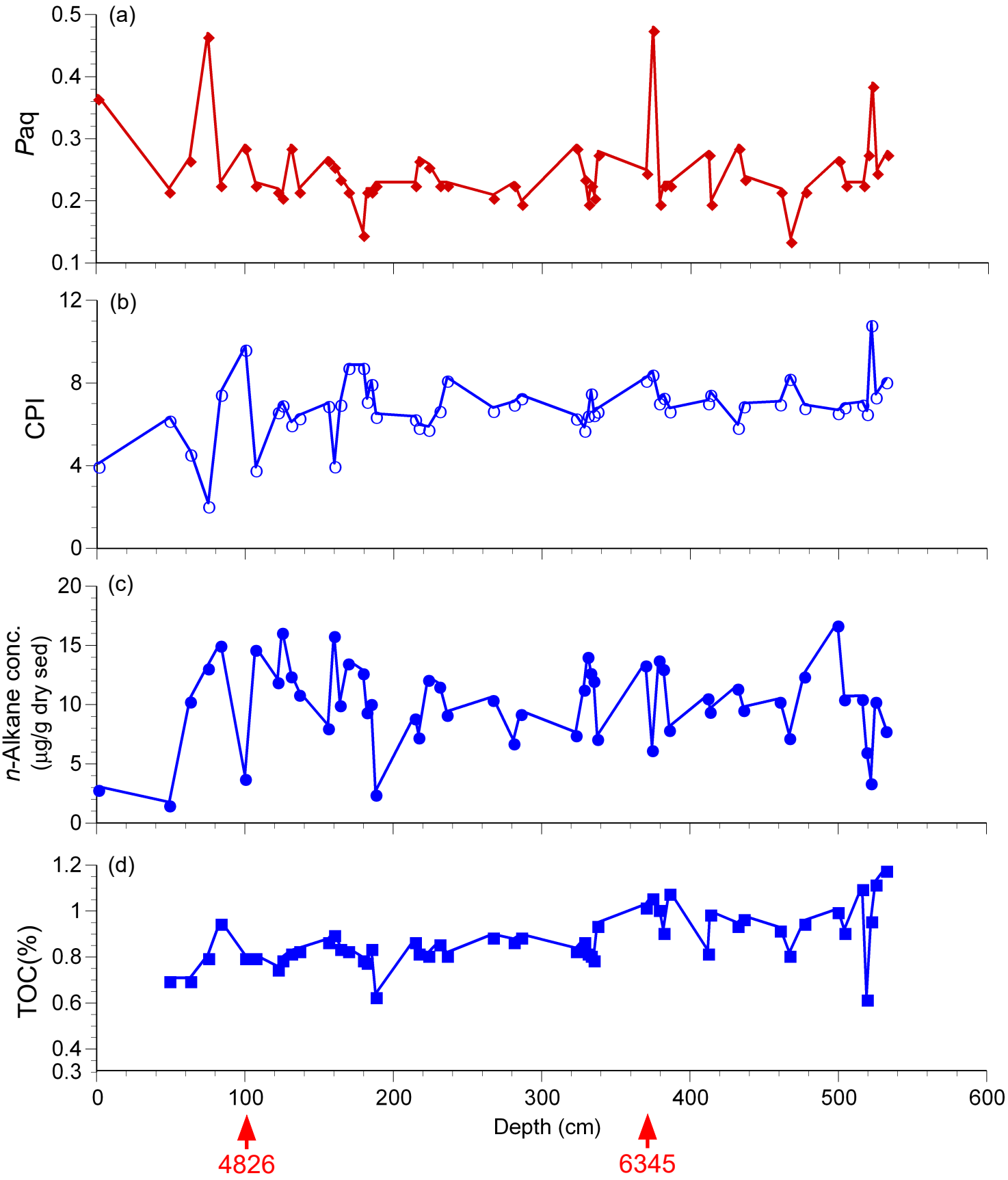

Figure 3 Depth profiles of the values of *n*-alkane proxies such as (a) aquatic macrophyte index (*P*aq) and (b) carbon preferential index (CPI), (c) total *n*-alkane concentrations, and (d) TOC in DBB samples of Dabusu Lake. Calendar ages are also shown.

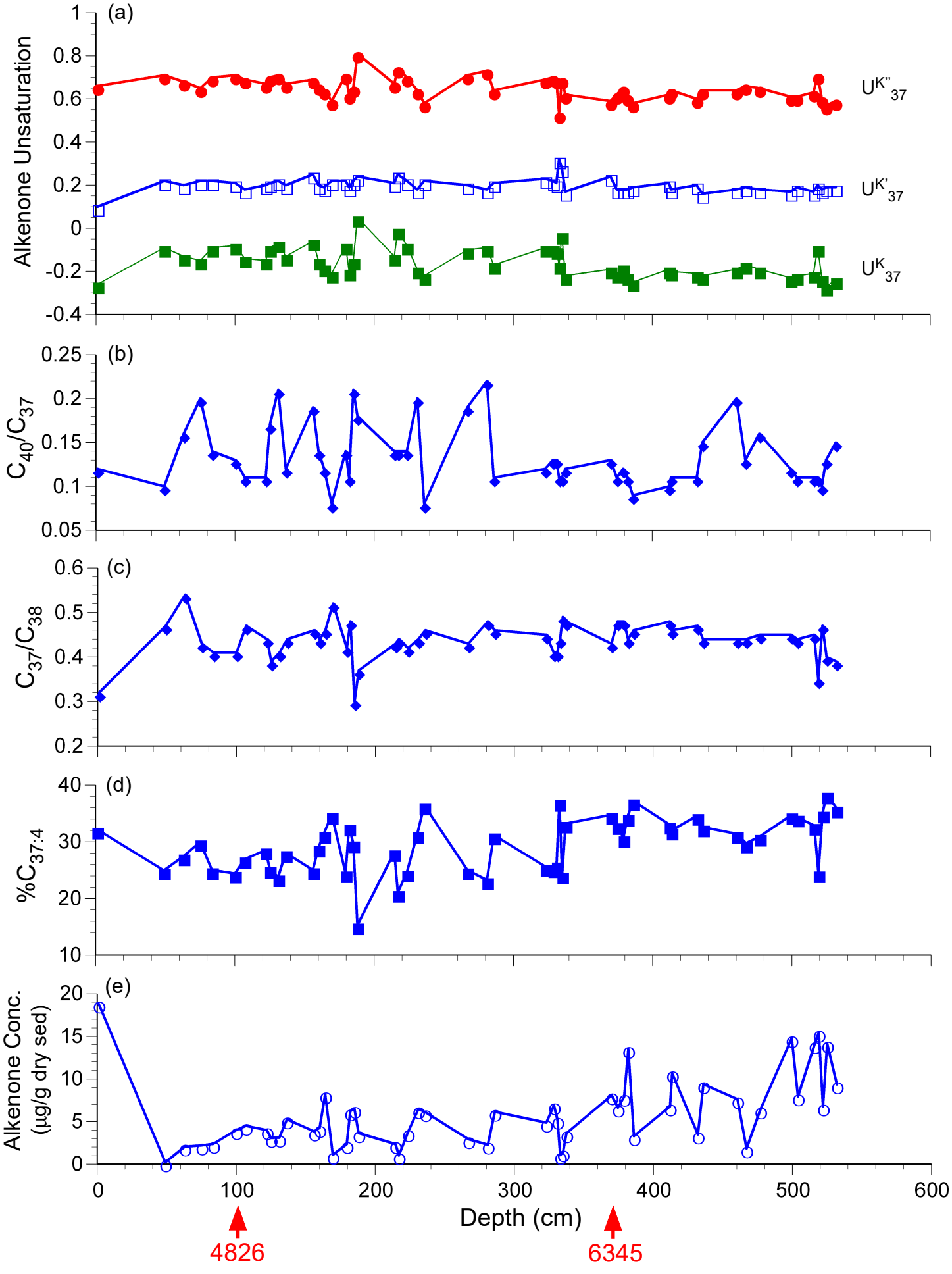

Figure 4 Depth profiles of (a) alkenone unsaturation indices (U^{K}_{37}, $U^{K'}_{37}$, and $U^{K''}_{37}$), chain length ratio of alkenones ((b) C_{40}/C_{37}, (c) C_{37}/C_{38}), (d) the percentage of $C_{37:4}$ alkenones ($\%C_{37:4}$), and (e) total alkenone concentrations. Calendar ages are also shown.

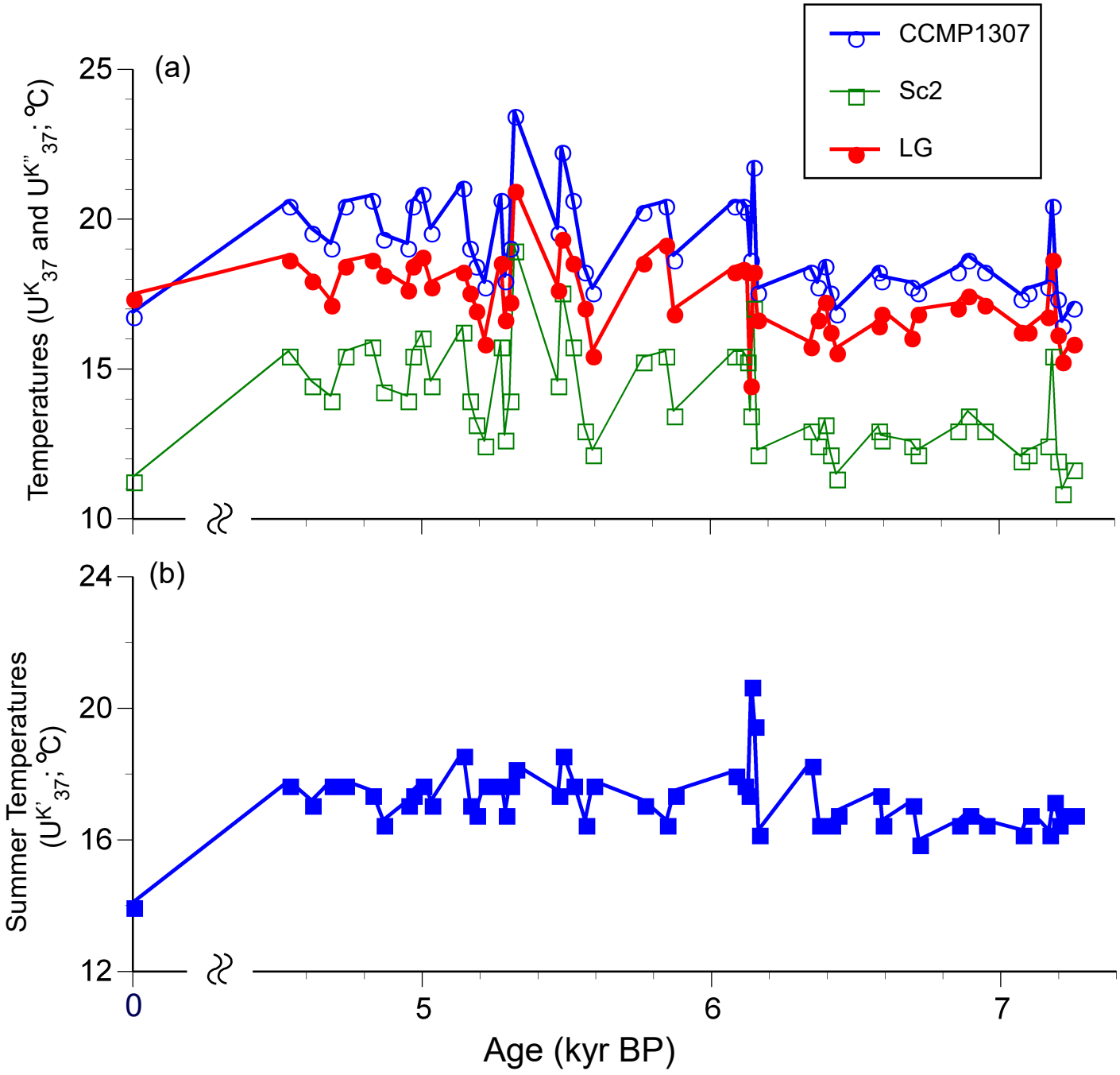

Figure 5 Age profiles of (a) variations in U^{K}_{37}-based water temperatures estimated using the calibrations obtained from *R. lamellosa* CCMP1307 (U^{K}_{37} = 0.045 T - 1.016; Nakamura et al., 2014) and *Isochrysis* Sc2 (Araie et al., 2018; U^{K}_{37} = 0.039 T - 0.70), as well as $U^{K''}_{37}$-based water temperatures estimated using the calibrations from *R. lamellosa* LG strain (U^{K}_{37} = 0.042 T - 0.08; Zhang et al., 2016), and (b) $U^{K'}_{37}$-based summer water temperatures calculated using the calibration of $U^{K'}_{37}$ of lacustrine sediments against the water temperatures of July in several Chinese lakes ($U^{K'}_{37}$ = 0.033 T - 0.367; Chu et al., 2005).

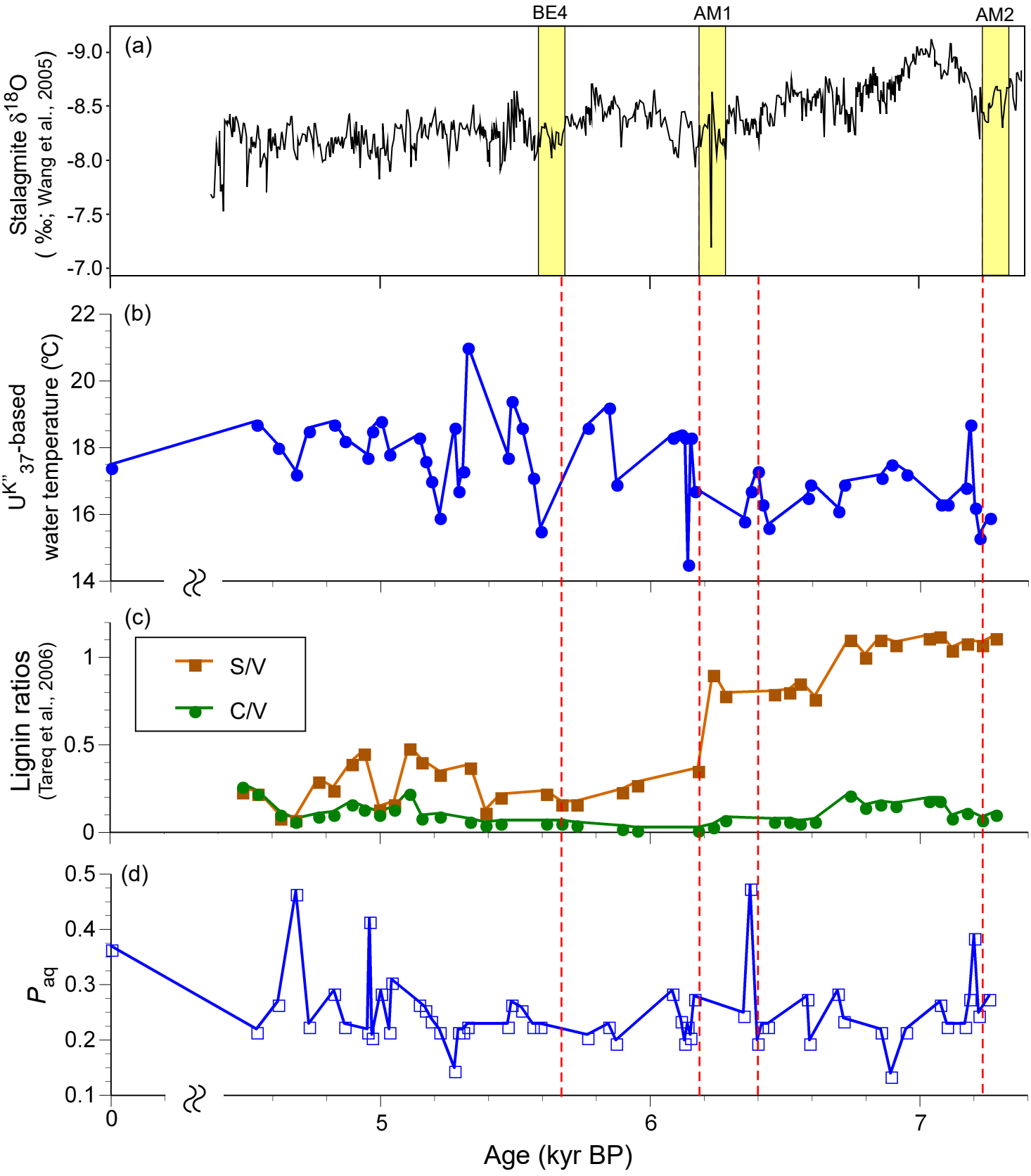

Figure 6 (a) Oxygen isotope ratio ($\delta^{18}O$) records in stalagmite of the Dongge Cave, southern China (Wang et al., 2005). AM 1 and AM 2 indicate Asian Monsoon events (Wang et al., 2005) and BE4 indicates Bond Event 4 (Bond et al., 2001). (b) Variations in $U^{K"}_{37}$-based water temperatures estimated using the calibration obtained from R. lamellosa LG strain ($U^{K"}_{37}$ = 0.045 T - 1.016; Zheng et al., 2014) in the DBB samples of Dabusu Lake. Paleovegetation records of a DBB core of Dabusu Lake; (c) variations in angiosperm / gymnosperm ratios estimated by the lignin ratios such as syringyl / vanillyl (S/V) and cinnamyl / vanillyl (C/V) ratios (Tareq et al., 2006), and (d) relative abundances of aquatic macrophytes estimated by Paq values in the DBB samples of Dabusu Lake.

Table 1 Data of total organic carbon content (TOC; %), concentrations of total n-alkanes and long chain alkenones (μg/g dry sediment) and the ratios of these compounds against TOC, *n*-alkane indicators such as carbon preferential index (CPI), average chain length (ACL), and aquatic plant n-alkane proxy (*P*aq) as well as alkenone proxies such as alkenone unsaturation indices (U^{K}_{37} and $U^{K'}_{37}$), the percentage of $C_{37:4}$ alkenones ($\%C_{37:4}$), chain length ratio of alkenones (C_{37}/C_{38} and C_{40}/C_{37}), as well as alkenone-based temperatures. $U^{K'}_{37}$-based summer (July) lake surface water temperatures calculated by the equations reported by Chu et al. (2005) (*1), $U^{K'}_{37}$-based water temperatures by the equations reported by Nakamura et al. (2012) (*2) and Araie et al. (2018) (*3), and $U^{K''}_{37}$-based water temperatures by the equations reported by Zhang et al. (2016) (*4). (See text).

Sample No.	Depth (cm)	Age (ka)	TOC (%)	Alkane conc. (μg/g dry sed)	Alkane /TOC	*n*-alkane proxies			Alkenone conc. (μg/g dry sed)	Alkenone /TOC	Alkenone proxies						Temperature (ºC)			
						CPI	ACL	P*aq*			U^{K}_{37}	$U^{K'}_{37}$	$U^{K''}_{37}$	$\%C_{37:4}$	C_{37}/C_{38}	C_{40}/C_{37}	Chu*1	CCMP1307*3	Sc2*4	LG*5
DBA1	1	0	0.61	1.85	3.03	6.53	28.47	0.28	14.33	23.49	-0.27	0.10	0.64	33.35	0.32	0.15	14.2	16.6	11.0	17.2
DBB-Pre	1	0	-	3.09	-	4.11	28.01	0.37	18.84	-	-0.26	0.10	0.66	32.20	0.32	0.12	14.1	16.9	11.4	17.5
DBB1	49	4.539	0.71	1.77	2.49	6.33	29.10	0.22	0.21	0.30	-0.09	0.22	0.71	24.97	0.47	0.10	17.8	20.6	15.6	18.8
DBB1-3	63	4.618	0.71	10.55	14.86	4.70	28.90	0.27	2.05	-	-0.13	0.20	0.68	27.46	0.54	0.16	17.2	19.7	14.6	18.1
DBB2	75	4.685	0.81	13.33	16.46	2.19	28.08	0.47	2.19	-	-0.15	0.22	0.65	29.97	0.43	0.20	17.8	19.2	14.1	17.3
DBB2-2	83.5	4.733	0.96	15.27	15.91	7.59	29.05	0.23	2.38	2.48	-0.09	0.22	0.70	25.06	0.41	0.14	17.8	20.6	15.6	18.6
DBB3-1	100	4.826	0.81	4.02	4.96	9.77	28.57	0.29	4.00	4.94	-0.08	0.21	0.71	24.42	0.41	0.13	17.5	20.8	15.9	18.8
DBB3-1-2	107	4.865	0.81	14.91	18.41	3.93	29.02	0.23	4.49	5.54	-0.14	0.18	0.69	26.94	0.47	0.11	16.6	19.5	14.4	18.3
DBB3-2-4	122	4.950	0.76	12.17	16.01	6.74	29.08	0.22	3.99	5.25	-0.15	0.20	0.67	28.54	0.44	0.11	17.2	19.2	14.1	17.8
DBB3-2-5	123.5	4.958	0.30	0.11	0.36	2.34	28.82	0.42	BL	-	-	-	-	-	-	-	-	-	-	-
DBB3-2-2	125	4.967	0.80	16.35	20.44	7.07	29.23	0.21	3.07	3.84	-0.09	0.21	0.70	25.27	0.39	0.17	17.5	20.6	15.6	18.6
DBB3-2	131	5.000	0.83	12.67	15.27	6.12	28.62	0.29	3.11	3.75	-0.07	0.22	0.71	23.78	0.41	0.21	17.8	21.0	16.2	18.9
DBB3-2-3	136.5	5.031	0.83	11.12	13.40	6.46	29.11	0.22	5.26	6.34	-0.13	0.20	0.67	28.06	0.44	0.12	17.2	19.7	14.6	17.9
DBB3-2-6	138	5.040	0.30	0.14	0.48	3.00	29.36	0.31	BL	-	-	-	-	-	-	-	-	-	-	-
DBB4-1	156	5.141	0.88	8.28	9.41	7.04	28.87	0.27	3.84	4.36	-0.06	0.25	0.69	25.04	0.46	0.19	18.7	21.2	16.4	18.4
DBB4-1-4	160	5.164	0.91	16.08	17.67	4.12	28.97	0.26	4.26	4.68	-0.15	0.20	0.66	28.97	0.44	0.14	17.2	19.2	14.1	17.7
DBB4-1-3	164	5.186	0.85	10.22	12.02	7.10	28.91	0.24	8.20	9.65	-0.18	0.19	0.64	31.47	0.46	0.12	16.9	18.6	13.3	17.1
DBB4-1-2	169.5	5.217	0.84	13.76	16.38	8.89	29.16	0.22	1.09	1.30	-0.21	0.22	0.59	34.81	0.52	0.08	17.8	17.9	12.6	16.0
DBB4-2-2	179.5	5.273	0.80	12.93	16.16	8.89	29.61	0.15	2.35	2.94	-0.08	0.22	0.71	24.51	0.42	0.14	17.8	20.8	15.9	18.7
DBB4-2-3	182	5.287	0.79	9.64	12.20	7.25	29.12	0.22	6.21	7.86	-0.20	0.19	0.62	32.70	0.48	0.11	16.9	18.1	12.8	16.8
DBB4-2	185	5.304	0.85	10.34	12.16	8.10	28.84	0.22	6.50	7.65	-0.15	0.22	0.65	29.76	0.30	0.21	17.8	19.2	14.1	17.4
DBB4-2-4	188	5.321	0.64	2.69	4.21	6.52	29.44	0.23	3.64	5.69	0.05	0.24	0.81	15.32	0.37	0.18	18.3	23.6	19.1	21.1
DBB5-1-2	214.5	5.470	0.88	9.12	10.36	6.39	29.03	0.23	2.36	2.68	-0.13	0.21	0.67	28.19	0.43	0.14	17.5	19.7	14.6	17.8
DBB5-1	217	5.484	0.83	7.51	9.05	5.99	28.91	0.27	1.02	1.23	-0.01	0.25	0.74	21.06	0.44	0.14	18.7	22.4	17.7	19.5
DBB5-2-2	223.5	5.521	0.82	12.37	15.09	5.90	28.59	0.26	3.75	4.57	-0.08	0.22	0.70	24.62	0.42	0.14	17.8	20.8	15.9	18.7
DBB5-2	231	5.563	0.87	11.80	13.56	6.80	28.87	0.23	6.46	7.43	-0.19	0.18	0.64	31.40	0.44	0.20	16.6	18.4	13.1	17.2
DBB5-2-3	236	5.591	0.82	9.42	11.49	8.27	28.95	0.23	6.10	7.44	-0.22	0.22	0.58	36.42	0.46	0.08	17.8	17.7	12.3	15.6
DBB6-1	267	5.766	0.90	10.67	11.86	6.81	29.16	0.21	2.93	3.26	-0.10	0.20	0.71	25.02	0.43	0.19	17.2	20.4	15.4	18.7
DBB6-2	281	5.844	0.88	7.01	7.97	7.11	29.04	0.23	2.28	2.59	-0.09	0.18	0.73	23.30	0.48	0.22	16.6	20.6	15.6	19.3
DBB6-2-2	286	5.872	0.90	9.49	10.54	7.42	29.26	0.20	6.15	6.83	-0.17	0.21	0.64	31.19	0.46	0.11	17.5	18.8	13.6	17.0
DBB7-2	323	6.081	0.84	7.68	9.14	6.44	28.81	0.29	4.87	5.80	-0.09	0.23	0.69	25.64	0.45	0.12	18.1	20.6	15.6	18.4
DBB7-2-3	328.5	6.112	0.88	11.54	13.11	5.86	29.02	0.24	6.91	7.85	-0.09	0.22	0.70	25.40	0.41	0.13	17.8	20.6	15.6	18.5
DBB7-2-5	331	6.126	0.83	14.32	17.25	6.57	29.26	0.20	5.22	6.29	-0.10	0.21	0.69	26.07	0.41	0.13	17.5	20.4	15.4	18.4
DBB7-2-2	333	6.137	0.82	12.94	15.78	7.64	29.01	0.23	1.07	1.30	-0.17	0.32	0.53	37.05	0.44	0.11	20.8	18.8	13.6	14.6
DBB7-2-6	335	6.148	0.80	12.27	15.34	6.61	29.25	0.21	1.38	1.73	-0.03	0.28	0.69	24.26	0.49	0.11	19.6	21.9	17.2	18.4
DBB7-2-4	337.5	6.162	0.95	7.38	7.77	6.78	28.78	0.28	3.62	3.81	-0.22	0.17	0.62	33.22	0.48	0.12	16.3	17.7	12.3	16.8
DBB8-2-4	370	6.345	1.03	13.59	13.19	8.27	28.89	0.25	8.08	7.84	-0.19	0.24	0.59	34.75	0.43	0.13	18.4	18.4	13.1	15.9
DBB8-2	374.5	6.370	1.07	6.43	6.01	8.56	27.97	0.48	6.64	6.21	-0.21	0.18	0.62	32.99	0.48	0.11	16.6	17.9	12.6	16.8
DBB8-2-3	379	6.396	1.02	14.03	13.75	7.18	29.27	0.20	7.91	7.75	-0.18	0.18	0.65	30.68	0.48	0.12	16.6	18.6	13.3	17.4
DBB8-2-5	382	6.413	0.92	13.27	14.42	7.43	29.02	0.23	13.52	14.70	-0.22	0.18	0.61	34.45	0.44	0.11	16.6	17.7	12.3	16.4
DBB8-2-2	386	6.435	1.09	8.15	7.48	6.79	28.89	0.23	3.29	3.02	-0.25	0.19	0.58	37.21	0.46	0.09	16.9	17.0	11.5	15.7
DBB9-1	412	6.581	0.83	10.81	13.02	7.18	28.86	0.28	6.78	8.17	-0.19	0.21	0.62	33.06	0.48	0.10	17.5	18.4	13.1	16.6
DBB9-1-2	413.5	6.590	1.00	9.68	9.68	7.58	29.22	0.20	10.68	10.68	-0.20	0.18	0.64	32.01	0.46	0.11	16.6	18.1	12.8	17.0
DBB9-2-2	432	6.694	0.95	11.63	12.24	5.99	28.85	0.29	3.48	3.66	-0.21	0.20	0.60	34.60	0.47	0.11	17.2	17.9	12.6	16.2
DBB9-2	436	6.716	0.98	9.82	10.02	7.03	29.06	0.24	9.38	9.57	-0.22	0.16	0.64	32.57	0.44	0.15	16.0	17.7	12.3	17.0
DBB10-1	460.5	6.854	0.93	10.52	11.31	7.12	28.94	0.22	7.62	8.19	-0.19	0.18	0.64	31.40	0.44	0.20	16.6	18.4	13.1	17.2
DBB10-1-2	467	6.891	0.82	7.45	9.09	8.36	29.54	0.14	1.83	2.23	-0.17	0.19	0.66	29.74	0.44	0.13	16.9	18.8	13.6	17.6
DBB10-2	477	6.947	0.96	12.64	13.17	6.95	29.20	0.22	6.42	6.69	-0.19	0.18	0.65	30.95	0.45	0.16	16.6	18.4	13.1	17.3
DBB10-3	499.5	7.074	1.01	16.96	16.79	6.70	28.91	0.27	14.79	14.64	-0.23	0.17	0.61	34.70	0.45	0.12	16.3	17.5	12.1	16.4
DBB10-3-3	504	7.099	0.92	10.72	11.65	6.99	29.03	0.23	7.95	8.64	-0.22	0.19	0.61	34.30	0.44	0.11	16.9	17.7	12.3	16.4
DBB10-3-2	516	7.166	1.11	10.75	9.68	7.10	29.15	0.23	14.09	12.69	-0.21	0.17	0.63	32.88	0.45	0.11	16.3	17.9	12.6	16.9
DBB10-3-4	519	7.183	0.63	6.26	9.93	6.66	29.49	0.28	15.44	24.50	-0.09	0.20	0.71	24.50	0.35	0.11	17.3	20.6	15.6	18.8
DBB10-4	522	7.200	0.97	3.64	3.75	10.95	28.35	0.39	6.76	6.97	-0.23	0.18	0.60	35.02	0.47	0.10	16.6	17.5	12.1	16.3
DBB10-4-3	525	7.217	1.13	10.53	9.32	7.46	28.91	0.25	14.14	12.51	-0.27	0.19	0.57	38.34	0.40	0.13	16.9	16.6	11.0	15.4
DBB10-4-2	532	7.256	1.19	8.04	6.76	8.20	28.71	0.28	9.36	7.87	-0.24	0.19	0.59	35.92	0.39	0.15	16.9	17.2	11.8	16.0